

Important note: The present paper work was sent to International Journal of Solids and Structures on 15 January 2018 (it is currently under review).

Octahedron family: the double-expanded octahedron tensegrity

Manuel Alejandro Fernández-Ruiz ^{a,*}; Enrique Hernández-Montes ^b; Juan Francisco Carbonell-Márquez ^c; Luisa María Gil-Martín ^d

^a Department of Structural Mechanics, University of Granada (UGR). Campus Universitario de Fuentenueva s/n. 18072 Granada, Spain. malejandrofr@ugr.es. *Corresponding author

^b Department of Structural Mechanics, University of Granada (UGR). Campus Universitario de Fuentenueva s/n. 18072 Granada, Spain. emontes@ugr.es.

^c Department of Mechanics, University of Córdoba. Campus de Rabanales, Edificio Leonardo da Vinci, E-14071 Córdoba, Spain. jcarbonell@uco.es.

^d Department of Structural Mechanics, University of Granada (UGR). Campus Universitario de Fuentenueva s/n. 18072 Granada, Spain. mlgil@ugr.es.

Abstract

The octahedron family of tensegrity structures is presented in this research. The octahedron and the expanded octahedron (well-known tensegrities in the literature) are the first and second components of the family. A new tensegrity is presented: the double-expanded octahedron. This new tensegrity form was obtained following the connectivity pattern of the octahedron family presented in this work. The values of the force densities or force:length ratios that satisfy the minimum required rank deficiency of the force density matrix were computed analytically. Two types of solutions are obtained: full and folded forms. Results show that each lower member of the octahedron family is a folded form of a superior member of this family. Several examples are shown.

Keywords: Tensegrity; Octahedron family; Analytical form-finding; Force density method.

1. Introduction

Tensegrity structures were first introduced by Fuller (Fuller, 1975). They have had a great development in the last years owing to their ingenious forms, lightweight, deployability and controllability. A tensegrity is defined as a prestressed discontinuous set of compression and tension members that are self-equilibrated. This type of structures is present in a wide diversity of fields as civil engineering (Adam and Smith, 2008), aerospace (Tibert and Pellegrino, 2002), biology (Ingber, 1998) and robotic (Graells Rovira and Mirats Tur, 2009). One of the key aspects in the design of tensegrity structures is to find a configuration of their members that leads to an equilibrium shape, process so-called form-finding.

Tibert and Pellegrino (Tibert and Pellegrino, 2003) presented a review of form-finding methods of tensegrity structures. One of these methods is the Force Density Method (FDM) proposed by Schek (Schek, 1974), which was originally conceived for the form-finding of tension only structures. The FDM is based on the concept of force:length ratio or force density q (Linkwitz and Schek, 1971; Schek, 1974) and it is widely used in the context of form-finding methods of tensegrity structures (Tran and Lee, 2010; Zhang and Ohsaki, 2006). Other alternative methods, such as the dynamic relaxation method introduced by Otter (Otter, 1965), can also be applied to the form-finding of tensegrity structures (Bel Hadj Ali et al., 2011; Zhang et al., 2006).

A challenge related to the design of tensegrity structures is the development of an analytical form-finding method with application to high-order tensegrity structures. There are many works related to numerical methods using FDM (Estrada et al., 2006; Masic et al., 2005; Tran and Lee, 2010; Zhang and Ohsaki, 2006) but little has been published in the literature about analytical methods (Hernández-Montes et al., 2017; Vassart and Motro, 1999; Zhang et al., 2013). The analytical method consists on

finding a set of force densities in a symbolic analysis that achieve an equilibrium shape of the tensegrity. In order to simplify the computation, some symmetric properties are considered. Indeed, symmetry of tensegrity structures has been a great source to obtain equilibrium configurations for form-finding methods (Masic et al., 2005).

The octahedron family is defined as a group of tensegrity structures which share the same connectivity pattern. Both the octahedron and the expanded octahedron (well-known tensegrity forms in the literature) belong to the so-called octahedron family as it is proved in the present work. In this work, the double-expanded octahedron is obtained following a certain connectivity pattern which is applicable to the members of the octahedron family. Due to their special characteristics, the members of the octahedron family can be used as modules in tensegrity domes, towers and bridges and as actuators or absorbers (expanded octahedron in (Xu and Luo, 2011)), as well as to many others potential applications. An analytical method is used to solve the form-finding problem obtaining both, full and folded forms (Hernández-Montes et al., 2017). Full forms are tensegrity structures where all the nodes in the equilibrium shape have different coordinates while in the folded forms some nodes share the same position in the equilibrium configuration. It is interesting to remark that the equilibrium shape of the double-expanded octahedron was not known a priori but it was obtained from the connectivity matrix which in turn depends on a connectivity pattern.

2. Equilibrium, rank deficiency and stability of tensegrity structures

2.1 Equilibrium of tensegrity structures

The equilibrium equations of a general mesh composed by $n + n_f$ nodes (being n the free nodes and n_f the fixed nodes) and m members are linearized by giving values of force:length ratios q to each member of the mesh (Linkwitz and Schek, 1971; Schek, 1974). The topology of the mesh is described by the connectivity matrix $C_s (\in \mathcal{R}^{m \times (n+n_f)})$ as discussed in (Hernández-Montes et al., 2006; Jurado-Piña

et al., 2009). If the member j connects nodes i and k ($i < k$), then the i th and k th elements of the j th row of \mathbf{C}_s are set to 1 and -1 respectively, as follows:

$$\mathbf{C}_s(j,r) = \begin{cases} +1 & \text{if } i(j)=r \\ -1 & \text{if } k(j)=r \\ 0 & \text{for the rest} \end{cases} \quad (1)$$

In Eq. (1), r denotes the r th column of the j th row in \mathbf{C}_s . The connectivity matrix can be partitioned into two parts as $\mathbf{C}_s = [\mathbf{C} | \mathbf{C}_f]$ if the free nodes are numbered first. In that case \mathbf{C} ($\in \mathfrak{R}^{m \times n}$) represents the connectivity of free nodes and \mathbf{C}_f ($\in \mathfrak{R}^{m \times n_f}$) represents the connectivity of the fixed nodes. In tension (Hernández-Montes et al., 2006) and compression structures (Fernández-Ruiz et al., 2017) where the q value of all the members is of the same sign and fixed nodes are present, the form-finding problem is well-solved (Levy and Spillers, 2004).

In the case of tensegrities some members are in tension ($q > 0$, cables) and others in compression ($q < 0$, struts) and because they are free-standing structures no supports exist (that is: $n_f = 0$). Accounting for this, the equilibrium equations of tensegrity structures can be formulated as (Schek, 1974; Tran and Lee, 2010):

$$\left. \begin{aligned} \mathbf{D} \cdot \mathbf{x} &= \mathbf{0} \\ \mathbf{D} \cdot \mathbf{y} &= \mathbf{0} \\ \mathbf{D} \cdot \mathbf{z} &= \mathbf{0} \end{aligned} \right\} \quad (2)$$

where $\mathbf{D} = \mathbf{C}^T \mathbf{Q} \mathbf{C}$ ($\in \mathfrak{R}^{n \times n}$) is the force density matrix and \mathbf{x} , \mathbf{y} and \mathbf{z} ($\in \mathfrak{R}^n$) are the nodal coordinate vectors of the nodes. The values of the force:length ratio of each member are collected in the vector $\mathbf{q} = (q_1, q_2, q_3, \dots, q_m)$ being \mathbf{Q} the diagonal square matrix of vector \mathbf{q} .

2.2 Rank deficiency

It can be proved that, in order to obtain a structure with dimension d , it is necessary that the rank deficiency of the force density matrix has to be at least $d + 1$ (Hernández-Montes et al., 2017), what is called non-degeneracy condition.

According to its definition ($\mathbf{D} = \mathbf{C}^T \mathbf{Q} \mathbf{C}$), matrix \mathbf{D} is a symmetric real matrix, so it is orthogonally diagonalizable by the spectral theorem: $\boldsymbol{\lambda} = \mathbf{P}^{-1} \mathbf{D} \mathbf{P}$, where $\boldsymbol{\lambda}$ is a diagonal matrix that contains all the eigenvalues of \mathbf{D} ($\lambda_1, \lambda_2, \lambda_3, \dots, \lambda_n$) and \mathbf{P} is an orthogonal matrix (that is $\mathbf{P}^{-1} = \mathbf{P}^T$) in which columns are an orthonormal base of eigenvectors of \mathbf{D} . By definition $\ker(\mathbf{D})$ is the eigenspace of eigenvalue 0, so the dimension of $\ker(\mathbf{D})$ coincides with the multiplicity of 0 as eigenvalue of \mathbf{D} . The eigenvalues of \mathbf{D} are the solution of the characteristic polynomial $p(\lambda)$ of \mathbf{D} , which has the form $p(\lambda) = \lambda^n + a_{n-1}\lambda^{n-1} + \dots + a_1\lambda + a_0$. The determinant of \mathbf{D} is always 0 since the row and column sums are zero and so $a_0 = 0$ (Hernández-Montes et al., 2017). As a consequence, a necessary condition for the development of a tensegrity in the space (three-dimensional, $d = 3$) is that: $a_1(q_1, \dots, q_m) = a_2(q_1, \dots, q_m) = a_3(q_1, \dots, q_m) = 0$. In this way, the characteristic polynomial is collected in the form $p(\lambda) = (\lambda^{n-4} + \dots + a_4)\lambda^4$, being 0 a solution of power λ^4 (which corresponds to a multiplicity of the eigenvalue 0 equal to $d + 1 = 4$). The condition $a_1(q_1, \dots, q_m) = a_2(q_1, \dots, q_m) = a_3(q_1, \dots, q_m) = 0$ is a system of polynomial equations in the force:length ratios q , which can be solved analytically if some relations between q values are imposed (Hernández-Montes et al., 2017).

2.3 Stability of tensegrity structures

This section is introduced in order to present this work in a self-contained format. In the following sections the study of the stability of the different equilibrium shapes presented herein are going to be analyzed. It is known that a tensegrity is stable if it returns to its equilibrium configuration after release of small enforced deformations or, in other words, any enforced deformation applied to a stable structure leads to an increase of its total potential energy. Mathematically the former condition implies that the potential energy has a minimum for the configuration for which the structure is stable.

Assuming linear elastic relationship between normal stresses and strains and accounting for the

definition of force:length ratio coefficient $\left(\sigma = \frac{N_k}{\Omega_k} = \frac{q_k L_k}{\Omega_k} = E \varepsilon \text{ with } \varepsilon = \frac{L_k - L_k^0}{L_k^0} \right)$, the axial load

acting in the member k of the tensegrity, N_k , can be expressed as:

$$N_k = E_k \cdot \Omega_k \cdot \varepsilon_k = E_k \cdot \Omega_k \cdot \frac{L_k - L_k^0}{L_k^0} \quad (3)$$

Being E_k and Ω_k the Young's modulus and the cross-sectional area and L_k and L_k^0 the final and initial lengths of the member k , respectively.

The elastic potential energy of a discrete structure of m members, such as a tensegrity, accounting Eq. (3) can be expressed as follow:

$$\begin{aligned} \Gamma_{st} &= \int_{Vol} \frac{1}{2} \sigma \varepsilon dVol = \frac{1}{2} \int_{L_0} \sigma \varepsilon \Omega dx = \frac{1}{2} \int_{L_0} \frac{N}{\Omega} \varepsilon \Omega dx = \frac{1}{2} \int_{L_0} N \varepsilon dx \rightarrow \\ \Gamma_{st} &= \frac{1}{2} \sum_{k=1}^m N_k \cdot \varepsilon_k \cdot L_k^0 = \frac{1}{2} \sum_{k=1}^m \frac{E_k \cdot \Omega_k \cdot (L_k - L_k^0)^2}{L_k^0} \end{aligned} \quad (4)$$

Using a Taylor series expansion in displacements, the deformation energy associated with a differential deformation of a tensegrity with n nodes and dimension d can be approximated by:

$$\Delta \Gamma_{st} \approx \sum_{i=1}^{dn} \frac{\partial \Gamma_{st}}{\partial \delta_i} d\delta_i + \frac{1}{2} \sum_{i=1}^{dn} \sum_{j=1}^{dn} \frac{\partial^2 \Gamma_{st}}{\partial \delta_i \partial \delta_j} d\delta_i d\delta_j \quad (5)$$

Being δ the vector of nodal coordinates:

$$\delta^T = \{ \mathbf{x}, \mathbf{y}, \mathbf{z} \} = \{ x_1, \dots, x_n, y_1, \dots, y_n, z_1, \dots, z_n \} \quad (6)$$

Therefore, if the equilibrium configuration of the tensegrity is to be stable, then $\Delta \Gamma_{st} > 0$.

It can be proved that if Eq. (4) is derived, the first term of the series in Eq. (5) corresponds to the equilibrium of the tensegrity:

$$\mathbf{A} \cdot \mathbf{q} = \mathbf{0} \text{ being } \mathbf{A} = \begin{pmatrix} \mathbf{C}^T \text{diag}(\mathbf{C} \cdot \mathbf{x}) \\ \mathbf{C}^T \text{diag}(\mathbf{C} \cdot \mathbf{y}) \\ \mathbf{C}^T \text{diag}(\mathbf{C} \cdot \mathbf{z}) \end{pmatrix} \quad (7)$$

with $\mathbf{A} \in \mathcal{R}^{d \times m}$ the equilibrium matrix of the tensegrity. As a result, the first term of the series in Eq.

(5) vanishes according to Eq. (7), that is:

$$\frac{\partial \Gamma_{st}}{\partial \delta_j} = \mathbf{A} \cdot \mathbf{q} = \mathbf{0} \quad (8)$$

Regarding the second term of the series in Eq. (5), it is evident that it corresponds to the derivative of the equilibrium condition:

$$\frac{1}{2} \sum_{i=1}^{dn} \sum_{j=1}^{dn} \frac{\partial^2 \Gamma_{st}}{\partial \delta_i \partial \delta_j} d\delta_i d\delta_j = \frac{1}{2} d\delta^\top \left[\frac{\partial}{\partial \delta_i} \left(\frac{\partial \Gamma_{st}}{\partial \delta_j} \right) \right] d\delta = \frac{1}{2} d\delta^\top \left[\frac{\partial}{\partial \delta_i} (\mathbf{A} \cdot \mathbf{q}) \right] d\delta \quad (9)$$

Accounting that:

$$\mathbf{A} \cdot \mathbf{q} = \begin{pmatrix} \mathbf{D} \cdot \mathbf{x} \\ \mathbf{D} \cdot \mathbf{y} \\ \mathbf{D} \cdot \mathbf{z} \end{pmatrix} \quad (10)$$

Operating and rearranging conveniently, the following expression is obtained:

$$d\delta^\top \left[\frac{\partial}{\partial \delta_i} (\mathbf{A} \cdot \mathbf{q}) \right] d\delta = d\delta^\top \left[\mathbf{A} \cdot \text{diag} \left(\frac{E_k \Omega_k}{(L_k^0)^3} \right) \cdot \mathbf{A}^\top + \mathbf{I}_3 \otimes \mathbf{D} \right] d\delta = d\delta^\top [\mathbf{K}_{\text{Elast}} + \mathbf{K}_{\text{Geom}}] d\delta \quad (11)$$

In Eq. (11) the symbol \otimes denotes tensor product (Kronecker product), $\mathbf{K}_{\text{Elast}}$ is the elastic stiffness matrix in the global coordinate system and \mathbf{K}_{Geom} is the geometric stiffness matrix or initial stress matrix when both small deformations and Green-Lagrange strain tensor are considered being invariable with respect to the coordinate system (Gil-Martín et al., 2017a, 2017b). As the condition $\frac{\partial \Gamma_{st}}{\partial \delta_i} = 0$ is always fulfilled because corresponds to the equilibrium condition (see Eq. (7) and Eq. (8)), the tensegrity is stable if the second term of $\Delta \Gamma_{st}$, Eq. (9), finally expressed in Eq. (11) is always positive for all the values of $d\delta$, vector of differential displacements of the nodes others than the rigid-body displacements, that is:

$$d\delta^\top [\mathbf{K}_{\text{Elast}} + \mathbf{K}_{\text{Geom}}] d\delta > 0 \quad (12)$$

The former inequality is true if the tangent stiffness matrix $\mathbf{K} = \mathbf{K}_{\text{Geom}} + \mathbf{K}_{\text{Elast}}$ is a positive semi-definite matrix.

Relevant intermediate steps from Eq. (5) to Eq. (11) have been included in Section A.1 of Appendix A.

Accounting that the compatibility matrix of the tensegrity is $\mathbf{L}^{-1}\mathbf{A}^T$ (see Section A.2 of Appendix A) the compatibility conditions in the structure corresponds to:

$$\mathbf{L}^{-1}\mathbf{A}^T \boldsymbol{\delta} = \boldsymbol{\Delta}\ell \quad (13)$$

Being $\boldsymbol{\delta}$ the vector of infinitesimal displacements of the nodes, $\mathbf{L} = \text{diag}(\mathbf{l})$ where \mathbf{l} is the vector containing the length of the members and $\boldsymbol{\Delta}\ell$ the vector containing the variations of lengths of the elements of the tensegrity.

If mechanisms are defined as non-trivial displacements, other than rigid-body motions, preserving the lengths of the members then if the increment displacement $d\boldsymbol{\delta}$ in Eq. (12) corresponds to a mechanism, $d\boldsymbol{\delta}_m$, according to Eq. (13) the term corresponding to the elastic stiffness matrix vanishes and the tensegrity is stable if:

$$d\boldsymbol{\delta}_m^T [\mathbf{I}_3 \otimes \mathbf{D}] d\boldsymbol{\delta}_m > 0 \quad (14)$$

which is true if the geometrical stiffness matrix is a positive-semidefinite matrix. This latter condition is called prestress-stability.

According to (Zhang and Ohsaki, 2007) a d dimensional tensegrity structure is super-stable if the following three conditions are all satisfied: *i.* The force density matrix \mathbf{D} has the minimum necessary rank deficiency $d + 1$ (see Section 2.2); *ii.* The force density matrix \mathbf{D} (or the geometric stiffness matrix, \mathbf{K}_{Geom}) is positive semi-definite, and *iii.* The member lengths of the structure are not changed by the non-trivial affine (infinitesimal) motions of the structure, or equivalently, the rank of the geometry matrix \mathbf{G} (see A.3 of Appendix A) is $d(d+1)/2$.

A deeper explanation of this section can be found in (Zhang and Ohsaki, 2015).

3. The octahedron family: connectivity pattern

The octahedron family is a group of tensegrity forms that share a common connectivity pattern. The first and simplest component of the family is the octahedron (see Figure 1.a), composed by 6 nodes and

15 members (3 struts and 12 cables). The second component of the family is the expanded octahedron (see Figure 1.b), which has 12 nodes and 30 members (6 struts and 24 cables). Both tensegrities are well-known tensegrity forms widely studied in the literature.

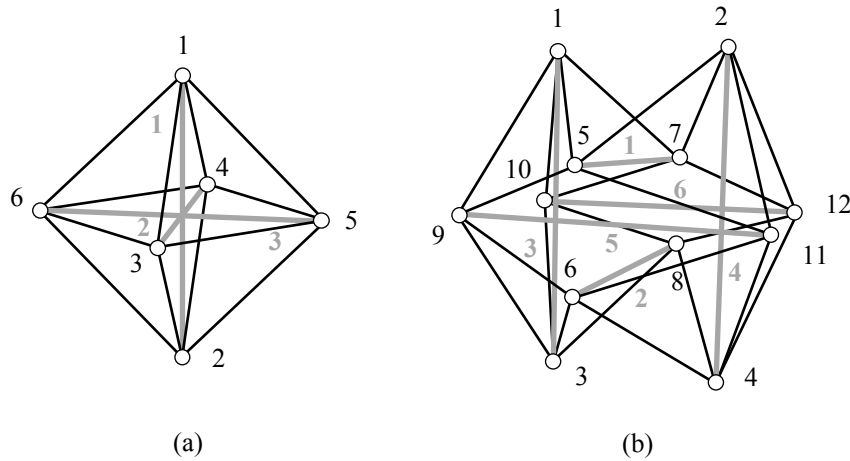


Figure 1. Octahedron (a) and expanded octahedron (b). Black lines correspond to cables and grey lines to struts. Black numbers correspond to nodes and grey numbers to struts, respectively.

In general, each individual of the octahedron family comes from the expansion of a previous member of the family. The name “expanded octahedron” itself indicates that it comes from the expansion of the octahedron in such a way that each node, cable and strut of the octahedron is duplicated during the expansion process.

All the components of the octahedron family can be obtained from the diamond pattern presented in (Pugh, 1976), that is, cables form diamonds or rhombic cells with a strut defining one diagonal, Figure 2.

It can be proved that each tensegrity of the octahedron family has as many rhombic cells as number of struts. A plane connection graph is the graphical representation of the connectivity between the nodes of each tensegrity. It is composed by rhombic cells connected among them and it is very useful for the construction of the connectivity matrix, C .

3.1. Connectivity rules

In order to obtain the graphical plane representations of the members of the octahedron family the following rules regarding the connectivity pattern need to be considered:

a) Each member of the family has twice the number of rhombic cells of the previous member of the family (and consequently twice the number of nodes, cables and struts).

b) Each node connects 4 cables and 1 strut (struts do not contact with each other, Figure 2).

c) Struts and cells are arranged in three groups.

In Figure 1.b, corresponding to the expanded octahedron, it can be seen that the pair of struts 1-2 comes from strut 2 of the octahedron (see Figure 1.a); analogously, the pairs of struts 3-4 and 5-6 in Figure 1.b come from struts 1 and 3 in Figure 1.a, respectively. Following the expansion pattern, one strut of the octahedron is the origin of two struts of the expanded octahedron and of four struts of the double-expanded octahedron. In general, all the struts of an upper member of this family will be overlapped in one strut of the octahedron (Figure 1.a) at the end of the folding process and so, because the octahedron has three struts, three groups of struts exist. Accordingly, the expanded octahedron (Figure 1.b) has three groups of struts with two struts per group. It is interesting to remark that, as there is a strut per cell there is an equivalence between strut and cell.

d) Nodes are arranged in pairs. Each pair of nodes is part of the same rhombic cell and they are not connected between them. This pair constitutes the principal nodes of the cell, being the other the secondary nodes (Figure 2). The principal nodes are called “top principal node” and “bottom principal node” so that they are numbered in order starting from the top.

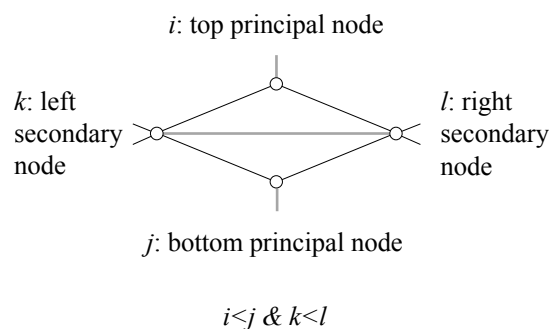


Figure 2. Rhombic cell and nomenclature of its nodes

The nodes of the expanded octahedron in Figure 1.b can be arranged in 6 pairs (1-2; 3-4; 5-6; 7-8; 9-10; 11-12). As in the case of the struts, a duplication of nodes occurs in the evolution from the

octahedron to the expanded octahedron: nodes 1 and 2 of the expanded octahedron come from node 1 of the octahedron in Figure 1.a. As can be seen in Figure 1.b in the rhombic cell defined by the nodes 1-7-2-5, the principal nodes 1-2 are not connected between them.

e) Each pair of nodes is connected with other pair of nodes through a pair of struts.

In Figure 1.b it can be seen that the pairs of nodes 1-2 and 3-4 are connected through the paired struts 3 and 4 in such a way that strut 3 links nodes 1 and 3 while strut 4 links nodes 2 and 4.

f) Each pair of nodes is connected through cables with other two nodes linked by a strut of another group.

For example, in Figure 1.b the pair of nodes 1-2 (which are linked to other nodes by two paired struts, 3 and 4) are connected through cables with the nodes 5-7, which are linked by the strut 1 (which is not part of the group of struts 3 and 4).

3.2. Graphical plane representation

Let us define p as the number that indicates the position of each tensegrity into the family (being $p = 1$ for the octahedron, $p = 2$ for the expanded octahedron and $p = 3$ for the tensegrity presented in this work which has been called as double-expanded octahedron). It can be proved that all of the previous rules are fulfilled for the members of the octahedron family up to the one corresponding to $p = 3$ if the plane representation graph of the member p is built as indicated below:

1- Draw a $3 \times 2^{(p-1)}$ matrix of rhombic cells so that the rows correspond to each group of cells (or struts).

For example, the octahedron has $3 \times 2^{(1-1)} = 3$ rhombic cells (see Figure 3.a). In this case, each group has only one rhombic cell and so each strut corresponds to a different group (see rule *c*).

2- Number consecutively only principal nodes of each rhombic cell.

See Figure 3.b. In this step, the pairs of nodes defined in rule *d*) are numbered.

3- Number the secondary nodes of each group of rhombic cells employing the numbers of the principal nodes corresponding to the next group following this particular protocol: firstly use in order

the number of the top principal nodes and secondly the corresponding to the bottom principal nodes.

Take into account that groups form a closed loop and so after group 3 is group 1 (Figure 3.c).

4- Construct the plane connection graph assembling the rhombic cells.

The plane connection graph of the octahedron is the one shown in Figure 3.d, which can be obtained matching the identical nodes in the rhombic cells in Figure 3.c, as if it was a puzzle. Arrows in Figure 3.d point out identical nodes in the graph.

Figure 3.d shows how the diamond cells need to be linked among them in order to get the 3D octahedron. It is evident that connectivity in Figure 3.d fulfils rules *b)*, *e)* and *f)*.

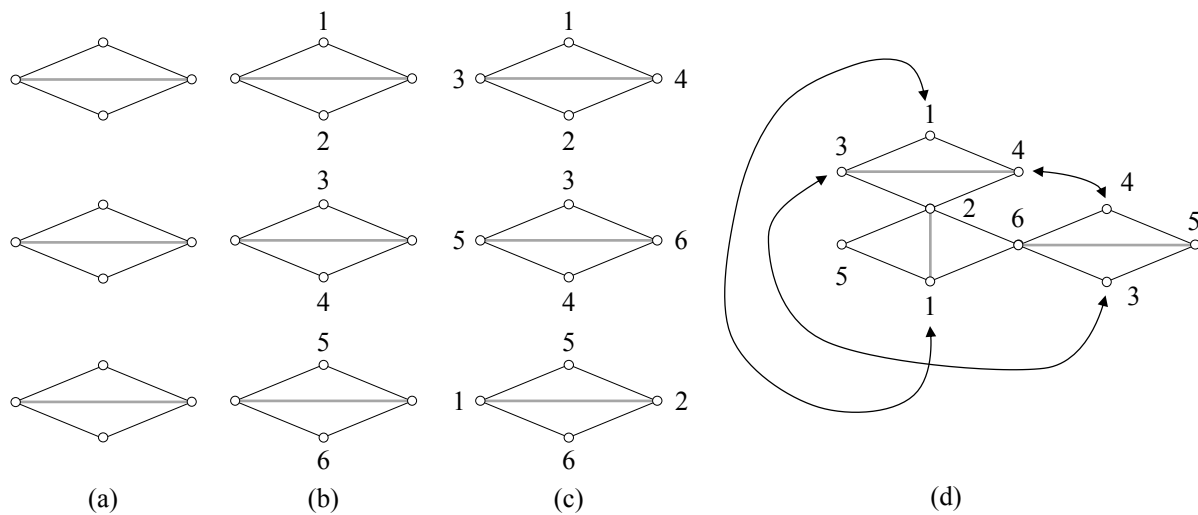


Figure 3. Plane connection graph of the octahedron. Black and grey lines correspond with cables and struts respectively. a) Rhombic cells, b) numbering of the not linked nodes, c) numbering of all nodes, d) connection graph.

In the case of the expanded octahedron ($p = 2$), there are $3 \times 2^{(2-1)} = 6$ rhombic cells arranged in three groups of two (Figure 4.a, 4.b and 4.c). The numbering of nodes and the plane connection graph corresponding to the expanded octahedron obtained according to the former connectivity rules is shown in Figure 4.b to 4.d. As in the previous case, arrows in Figure 4.d indicate the correspondence between identical nodes.

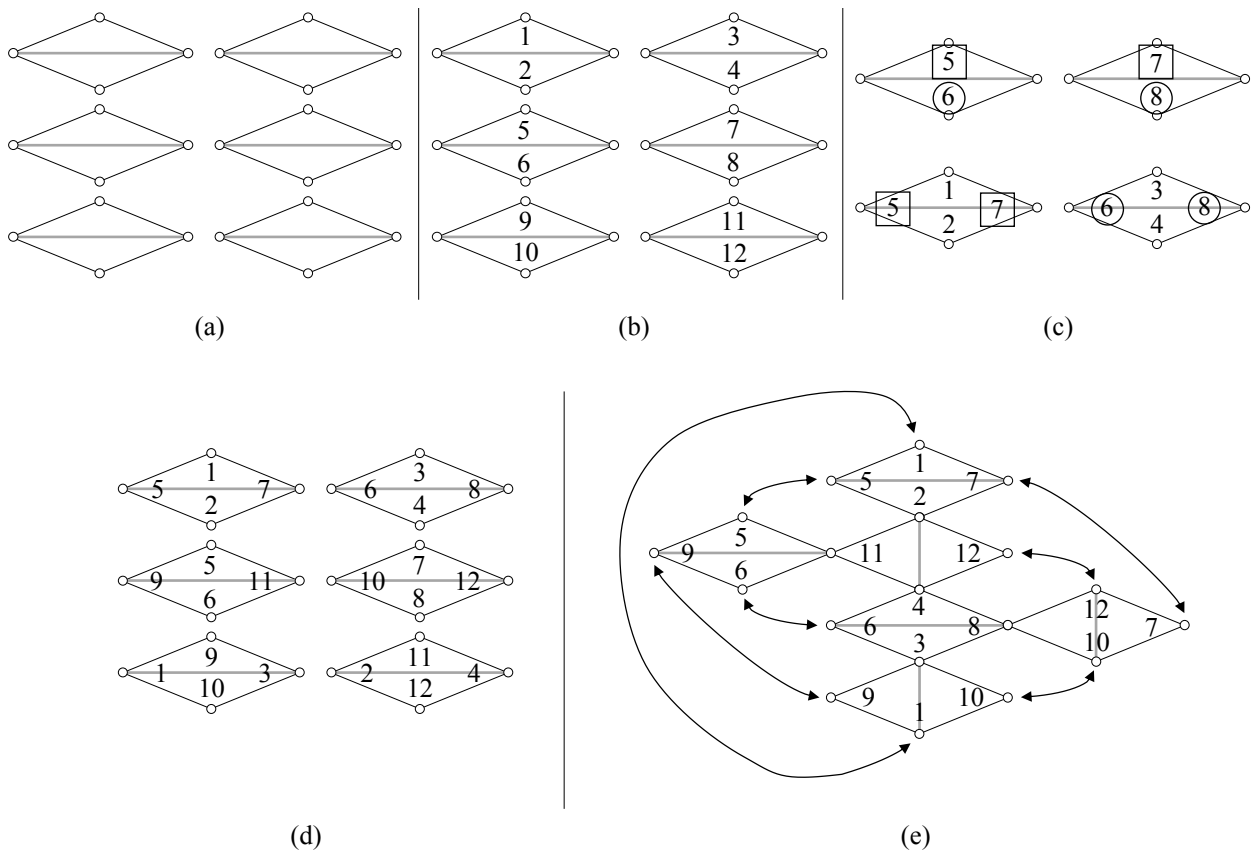


Figure 4. Plane connection graph of the expanded octahedron. Black and grey lines correspond with cables and struts respectively. a) Rhombic cells arranged in three groups, b) numbering of the not linked nodes, c) detail of step 3 in the numbering procedure, d) numbering of all nodes, d) connection graph.

Finally, the double-expanded octahedron ($p = 3$) has $3 \times 2^{(3-1)} = 12$ rhombic cells arranged in groups of three (with four cells per group). Both the plane connection graphs as well as the numbering of the nodes are shown in Figure 5 (the corresponding author, by request, will provide the connectivity matrix **C** of all the plane connection graphs shown in this work).

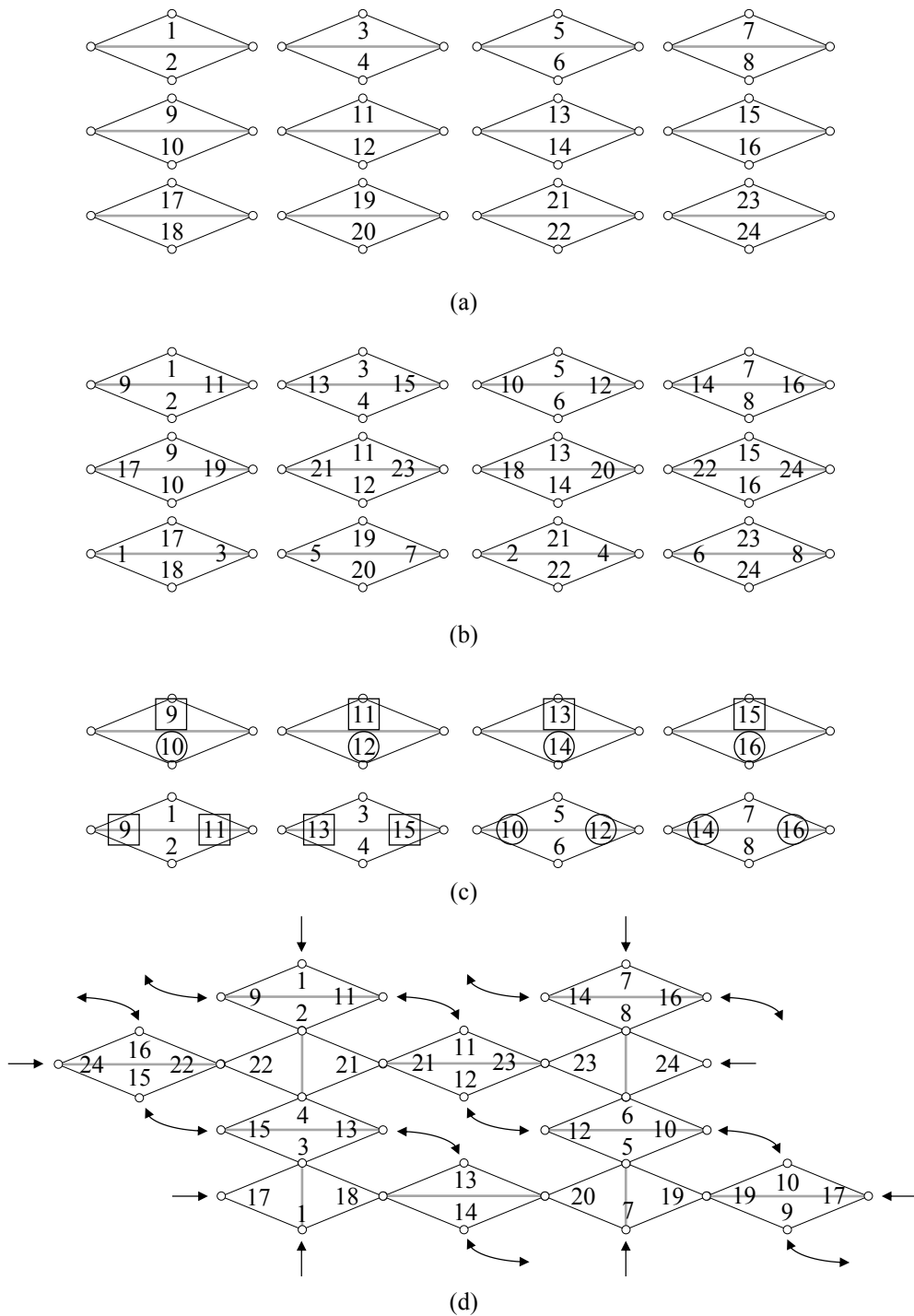


Figure 5. Plane connection graph of the double-expanded octahedron. a) Numbering of the not linked nodes of the rhombic cells arranged in three groups, b) numbering of all nodes, c) detail of step 3 in the numbering procedure, d) connection graph.

The former numbering procedure is valid for tensegrity structures of the octahedron family up to $p = 3$ due to the complexity of rule *f*) for higher members. The interaction between pairs of nodes and groups of struts change for each member and the proposed numbering procedure is not able to obtain the plane

connection graph bigger than $p = 3$ because it does not allow to link more than four cells per group. So, more research is needed in order to obtain higher superior members of this family, if they exist.

4. The octahedron family: form-finding

4.1 Octahedron

The equilibrium shape of the octahedron is obtained solving Eq. (2). The connectivity matrix $\mathbf{C} \in \mathfrak{R}^{15 \times 6}$ is obtained from the plane connection graph in Figure 3.d and it is defined according to Eq. (1). Only two force:length ratios are considered: q_1 for cables (black lines in Figure 3.d) and q_2 for struts (grey lines in Figure 3.d), resulting in a diagonal matrix $\mathbf{Q} \in \mathfrak{R}^{15 \times 15}$. Then the characteristic polynomial $p(\lambda)$ of matrix $\mathbf{D} \in \mathfrak{R}^{6 \times 6}$ is computed and the non-degeneracy condition in 3D leads to the system of equations $a_1(q_1, q_2) = a_2(q_1, q_2) = a_3(q_1, q_2) = 0$. The expressions of the polynomials a_1 , a_2 and a_3 are shown in Appendix B in Eqs. (B1), (B2) and (B3) respectively. The former equation system implies $\ker(\mathbf{D}) = 4$ as it has been explained in Section 2.2. This system has two possible solutions: $q_1 = q_2 = 0$ (not considered) and $q_2 = -2q_1$. For the latter solution, \mathbf{D} and the eigenvectors corresponding to the eigenvalue 0 (base of $\ker(\mathbf{D})$) are calculated and the coordinates of the nodes are obtained as a linear combination of these eigenvectors (see Figure 6).

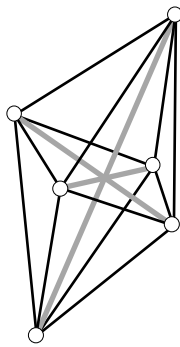


Figure 6. Final equilibrium shape of the octahedron. Black lines correspond with cables and grey lines with struts.

4.2 Expanded octahedron

As before, the connectivity matrix of the expanded octahedron $\mathbf{C} \in \mathfrak{R}^{30 \times 12}$ is obtained from its plane connection graph (Figure 4.d). Again, two values of the force:length ratio, q , are considered: q_1 for

cables (black lines in Figure 4.d) and q_2 for struts (grey lines in Figure 4.d), resulting in $\mathbf{Q} \in \mathfrak{R}^{30 \times 30}$. The characteristic polynomial $p(\lambda)$ of $\mathbf{D} \in \mathfrak{R}^{12 \times 12}$ is calculated and the system of equations $a_1(q_1, q_2) = a_2(q_1, q_2) = a_3(q_1, q_2) = 0$ solved (a_1 , a_2 and a_3 are shown in Appendix B in Eqs. (B4), (B5) and (B6) respectively), obtaining the following solutions: $q_1 = 0$ (not considered), $q_2 = -2q_1$ and $q_2 = -3/2q_1$. The first considered solution corresponds to the octahedron (see Figure 7.a) but, in this case, there are two nodes at the same position in the space (that is, duplicated) and that is why it is called a folded form (Hernández-Montes et al., 2017). The other solution, $q_2 = -3/2q_1$, corresponds to the expanded octahedron (see Figure 7.b) which is a full form (Hernández-Montes et al., 2017) since all the nodes of the resultant equilibrium shape have different coordinates one to one. The latter solution agrees with the solution obtained analytically by Tibert and Pellegrino (Tibert and Pellegrino, 2003) and numerically by Gómez-Estrada et al. (Estrada et al., 2006). So, based on the former result, it can be concluded that the octahedron is a folded form of the expanded octahedron.

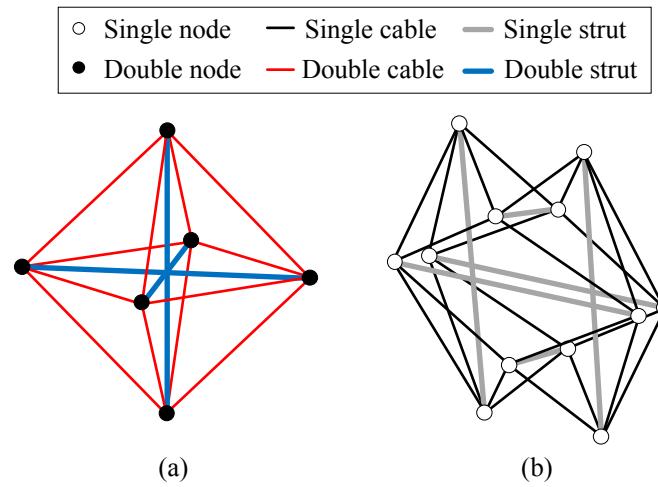


Figure 7. Equilibrium shapes of the octahedron (a) and the expanded octahedron (b) from graph in Figure 4.d. (For interpretation of the references to color in this figure legend, the reader is referred to the web version of this article).

Intermediate equilibrium configurations between the octahedron and the expanded octahedron (Figure 7.a and 7.b) can be obtained if three values of q are considered instead of two: q_1 for all the cables (black lines in Figure 4.d), q_2 for one group of struts (for example, members connecting nodes 5-7 and 6-8 in Figure 4.d) and q_3 for the other two groups of struts. The polynomials $a_1(q_1, q_2, q_3)$, $a_2(q_1, q_2, q_3)$ and $a_3(q_1, q_2, q_3)$ are not shown due to its length. In this case, seven solutions are obtained when the

non-degeneracy condition $\ker(\mathbf{D}) = 4$ is imposed: (1) $q_1 = 0$, (2) $q_1 = q_2 = 0$, (3) $q_1 = q_3 = 0$, (4) $q_2 = q_3 = -2q_1$, (5) $q_2 = q_3 = -3/2q_1$, (6) $q_2 = -2q_1$ & $q_3 = -3/2q_1$ and (7) $q_2 = -3/2q_1$ & $q_3 = -2q_1$. The first three solutions are not considered and the equilibrium configurations corresponding to the other solutions are depicted in Figure 8.

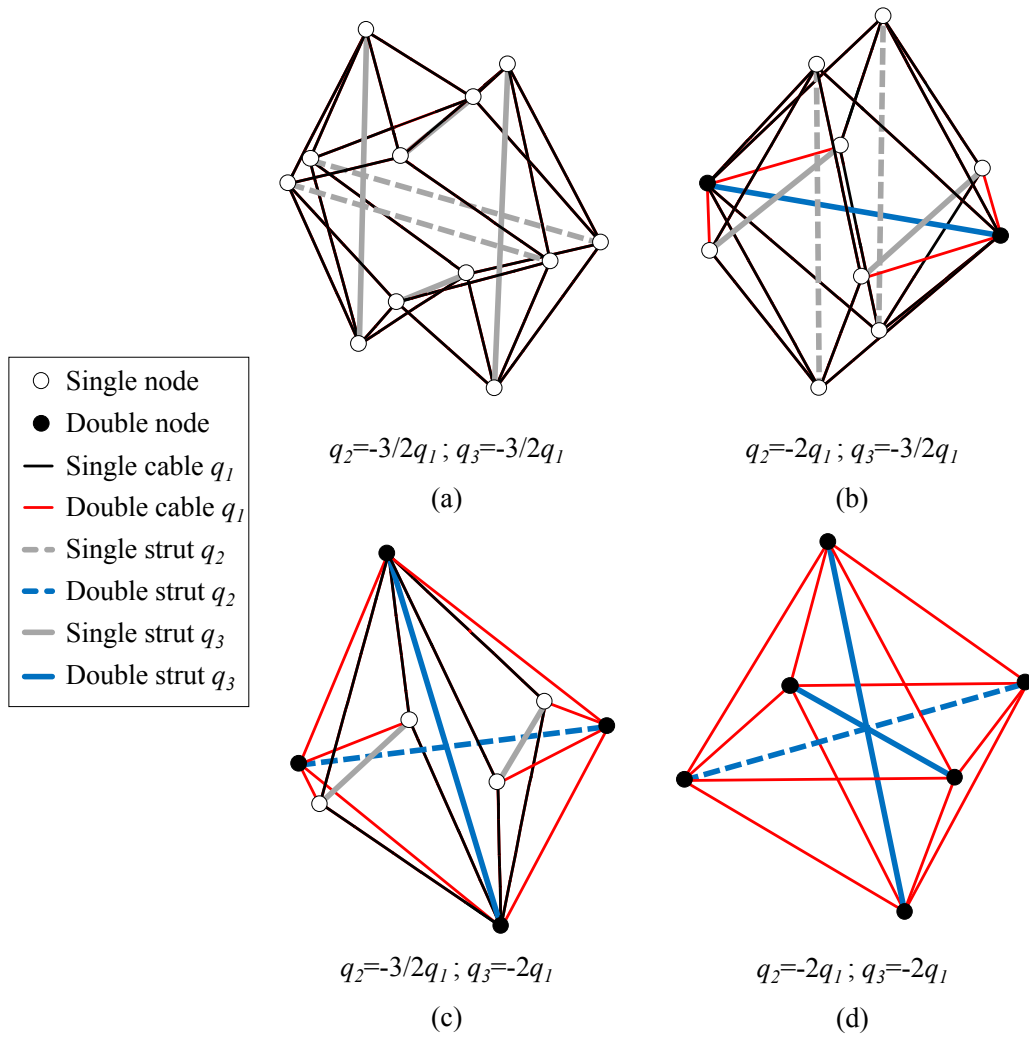


Figure 8. Equilibrium shapes obtained from the plane connection graph shown in Figure 4.d considering three different values of q . (a) Expanded octahedron, (b) intermediate state corresponding to $q_2 = -2q_1$ & $q_3 = -3/2q_1$, (c) intermediate state corresponding to $q_2 = -3/2q_1$ & $q_3 = -2q_1$, (d) octahedron. (For interpretation of the references to color in this figure legend, the reader is referred to the web version of this article).

In Figure 8, the only full form is the expanded octahedron (Figure 8.a). It can be seen that the folded forms depicted in Figure 8.b and Figure 8.c are intermediate states in the folding process from the expanded octahedron to the octahedron (Figure 8.d). Members and nodes overlapped at each equilibrium configuration are indicated in Figure 8.b to 8.d with different colour lines and black points,

respectively. Videos of tensegrity structures shown in Figure 8 are included as Supplementary Material.

4.3 Double-expanded octahedron

As well as the octahedron ($p = 1$) is a folded form of the expanded octahedron ($p = 2$, see Figure 8), the expanded octahedron itself is a folded form of a superior member of the family ($p = 3$). The presented double-expanded octahedron is a tensegrity which has not been studied up to now in the literature. The connectivity matrix $\mathbf{C} \in \mathfrak{R}^{60 \times 24}$ has been defined using the plane connection graph shown in Figure 5.c, which has been obtained following the connectivity pattern of the octahedron family presented in Section 3.

As in the previous cases only two values of the force:length coefficients are considered: q_1 for cables (black lines in Figure 5.c) and q_2 for struts (grey lines in Figure 5.c), resulting in $\mathbf{Q} \in \mathfrak{R}^{60 \times 60}$. Once the characteristic polynomial $p(\lambda)$ of $\mathbf{D} \in \mathfrak{R}^{24 \times 24}$ is calculated and the system of equations $a_1(q_1, q_2) = a_2(q_1, q_2) = a_3(q_1, q_2) = 0$ solved (a_1, a_2 and a_3 are shown in Appendix B in Eqs. (B7), (B8) and (B9) respectively) the following four solutions are obtained: (1) $q_1 = 0$ (not considered), (2) $q_2 = -2q_1$, (3) $q_2 = -3/2q_1$ and (4) $q_2 = -4/3q_1$. It can be proved that the solution $q_2 = -2q_1$ corresponds to the octahedron with all its members and nodes quadruplicated whereas than the solution $q_2 = -3/2q_1$ correspond to the expanded octahedron with all its members and nodes duplicated. Finally, the solution $q_2 = -4/3q_1$ corresponds to the double-expanded octahedron represented in Figure 9. A video is included in the Supplementary Material to better visualise the double-expanded octahedron final shape. In addition to this, a video constructing a real model of the double expanded octahedron is also included in the Supplementary Material.

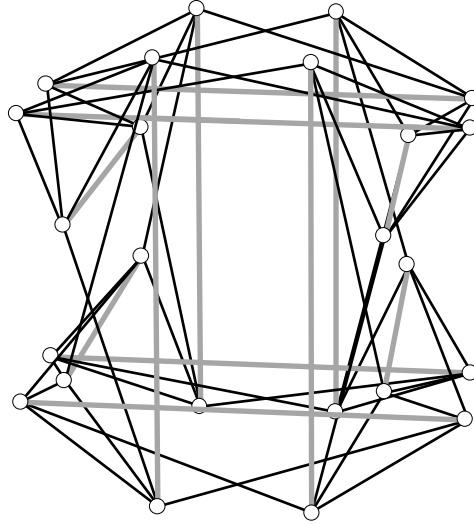


Figure 9. Double-expanded octahedron obtained from graph in Figure 5.c.

So, both the octahedron and the expanded octahedron are folded forms of the double-expanded octahedron, proving that the tensegrity structure shown in Figure 9 is the third component of the so-called octahedron family.

As in the case of the expansion from the octahedron to the expanded octahedron (Figure 8), intermediate states can be obtained if three (instead of two) different values of the force:length ratios are considered: q_1 for all the cables (black lines in Figure 5.d), q_2 for a group of struts (for example, members connecting nodes 9-11, 13-15, 10-12 and 14-16 in Figure 5.d) and q_3 for the other two groups of struts. As in the expanded octahedron case, polynomials $a_1(q_1, q_2, q_3)$, $a_2(q_1, q_2, q_3)$ and $a_3(q_1, q_2, q_3)$ are not shown due to its length. The following solutions are obtained: (1) $q_1 = 0$, (2) $q_1 = q_2 = 0$, (3) $q_1 = q_3 = 0$, (4) $q_2 = q_3 = -2q_1$, (5) $q_2 = q_3 = -3/2q_1$, (6) $q_2 = q_3 = -4/3q_1$, (7) $q_2 = -2q_1$ & $q_3 = -3/2q_1$, (8) $q_2 = -3/2q_1$ & $q_3 = -2q_1$, (9) $q_2 = -3/2q_1$ & $q_3 = -4/3q_1$ and (10) $q_2 = -4/3q_1$ & $q_3 = -3/2q_1$. The first three solutions are not considered. Solutions (4), (5) and (6) correspond to the octahedron, the expanded octahedron and the double-expanded octahedron, respectively; being the two first solutions folded forms and the last one the full form of the tensegrity. Solutions (7) and (8) correspond to intermediate states in the folding process from the expanded octahedron to the octahedron, both folded forms (see Figure 8.b and 8.c, respectively). The two last solutions correspond to intermediate states in the folding process from the double-expanded octahedron to the expanded octahedron and its

equilibrium configuration have been represented in Figure 10.b and 10.c, respectively. Videos of tensegrity structures shown in Figure 10 are included as Supplementary Material.

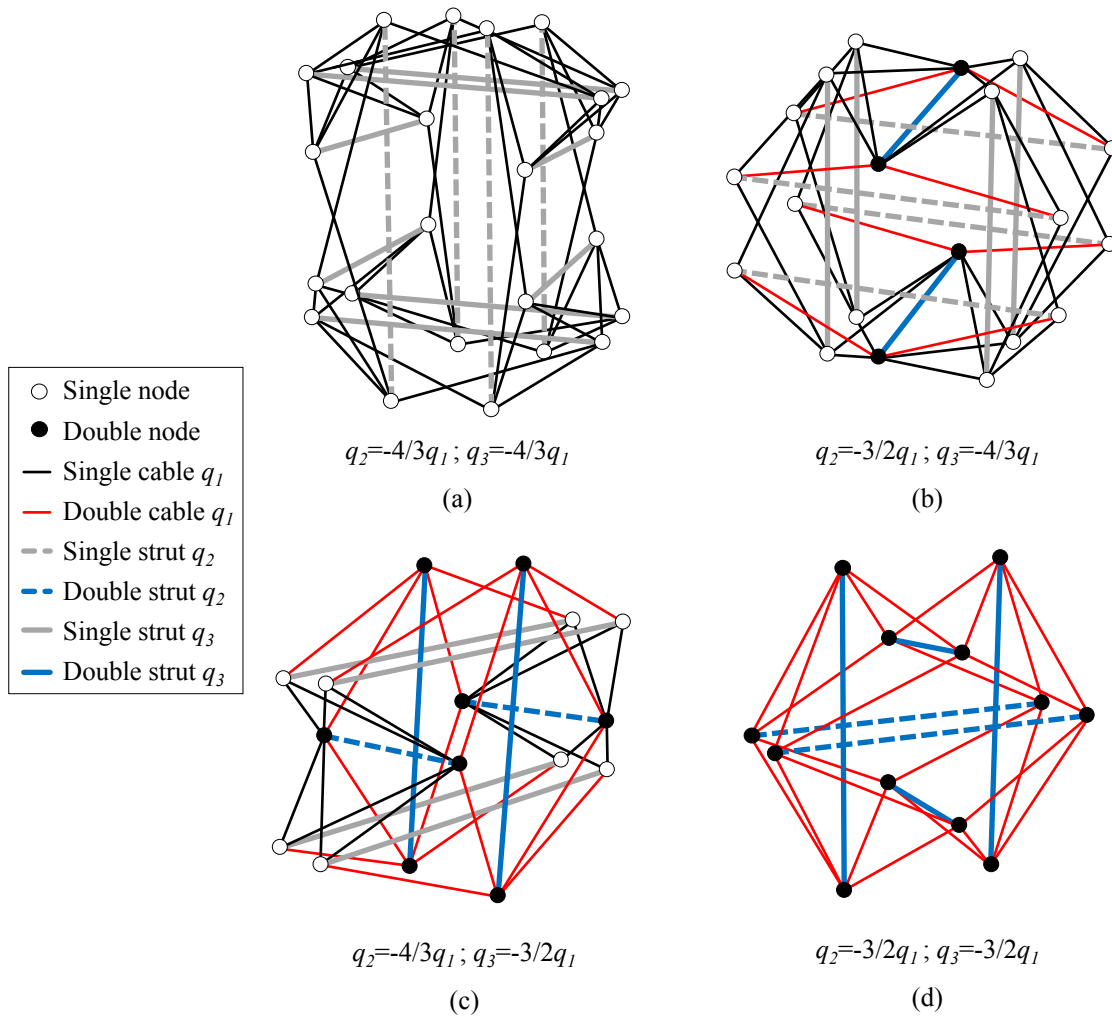


Figure 10. Equilibrium shapes obtained from the plane connection graph in Figure 5.d considering three different values of q . (a) Double-expanded octahedron, (b) intermediate state corresponding to $q_2 = -3/2q_1$ & $q_3 = -4/3q_1$, (c) intermediate state corresponding to $q_2 = -4/3q_1$ & $q_3 = -3/2q_1$, (d) expanded octahedron. (For interpretation of the references to color in this figure legend, the reader is referred to the web version of this article).

4.4 Stability of the octahedron family

In this section the stability of the tensegrities shown in Figure 8 and Figure 10 is studied. The cross-sectional areas and the material properties of the elements (cables and struts) and the level of prestress have to be known to analyse the stability but this information is not necessary in order to study the super-stability (Zhang and Ohsaki, 2015). For the sake of simplicity, the maximum force:length ratio

for all the elements (cables and struts) has been taken as 1% of the product $E\Omega$ (where Ω is the cross-sectional area of the member) as in (Zhang and Ohsaki, 2015).

The coordinates of the nodes are obtained using directly the eigenvectors corresponding to the $d + 1$ zero eigenvalues. As it has been shown in Section 2.2, the row and column sums of \mathbf{D} are zero, so vector $[1, 1, 1, \dots]$ is always solution of Eq. (2) (and consequently it is the corresponding eigenvector of a zero eigenvalue). Estrada et al. (Estrada et al., 2006) avoid this vector because it adds little information for the nodal coordinates. For this reason and without loss of generality in this work the other d eigenvectors are taken as the nodal coordinates of the tensegrity.

Table 1 shows, for the studied connectivity patterns, the full and folded forms of the members of the octahedron family which have been obtained using the analytical method to solve the form-finding problem. The corresponding values of the force:length ratios, the values of $\ker(\mathbf{D})$ and the stability classification of each tensegrity (Eq. (12) and Eq. (14)) have also been summarized. It can be proved that the condition *iii* (see Section 2.3) defined by (Zhang and Ohsaki, 2007) is fulfilled in all the cases studied in this paper because the rank of the structural geometry matrix is 6 (see A.3 Appendix A).

Table 1. Stability of the first three members of the octahedron family

Pattern	Double-expanded octahedron	Expanded octahedron	Octahedron
$n = 24$ $m = 60$ (Figure 5)	$q_2 = q_3 = -4/3q_1$ Full form $\ker(\mathbf{D}) = 4$ Super-stable	$q_2 = q_3 = -3/2q_1$ Folded form duplicated members and nodes $\ker(\mathbf{D}) = 4$ Unstable	$q_2 = q_3 = -2q_1$ Folded form quadruplicated members and nodes $\ker(\mathbf{D}) = 7$ Unstable
$n = 12$ $m = 30$ (Figure 4)	–	$q_2 = q_3 = -3/2q_1$ Full form $\ker(\mathbf{D}) = 4$ Super-stable	$q_2 = q_3 = -2q_1$ Folded form duplicated members and nodes $\ker(\mathbf{D}) = 4$ Unstable
$n = 6$ $m = 15$ (Figure 3)	–	–	$q_2 = q_3 = -2q_1$ Full form $\ker(\mathbf{D}) = 4$



All the full forms of the family (octahedron Figure 4, expanded octahedron Figure 8.a and double expanded octahedron Figure 9) are super-stable according to (Zhang and Ohsaki, 2015). On the other hand, folded forms shown in Figure 8.d and Figure 10.d (duplicated members and nodes) are unstable taking into account the materials properties and the level of prestress indicated above.

Now the stability and super-stability of the intermediate equilibrium configurations between the octahedron and the expanded octahedron (Figure 8.b and 8.c) and between the expanded octahedron and the double-expanded octahedron (Figure 10.b and 10.c) respectively are studied. Stability is analysed by means of the minimum eigenvalue of \mathbf{K} for each configuration and super-stability is accounted taking into consideration the minimum eigenvalue of matrix \mathbf{D} or, equivalently, \mathbf{K}_{Geom} (ii condition according to (Zhang and Ohsaki, 2007)). As the eigenvalues depends on a particular realisation of the matrices, a range of values for q_1 (in the same way for $q_2=f(q_1)$ and $q_3=f(q_1)$) is considered. Figure 11 shows those minimum eigenvalues for each tensegrity structure as a function of q_1 . The minimum eigenvalue of \mathbf{D} is always negative in all the intermediate equilibrium configurations studied so none of them can be considered super-stable. However, the minimum eigenvalue of \mathbf{K} in the tensegrities shown in Figure 8.b and Figure 10.b is zero and in the case of tensegrities shown in Figure 8.c and Figure 10.c is negative (see Figure 11). For these reasons, tensegrities in Figure 8.c and Figure 10.c are unstable and the tensegrities in Figure 8.b and Figure 10.c are stable but not super-stable.

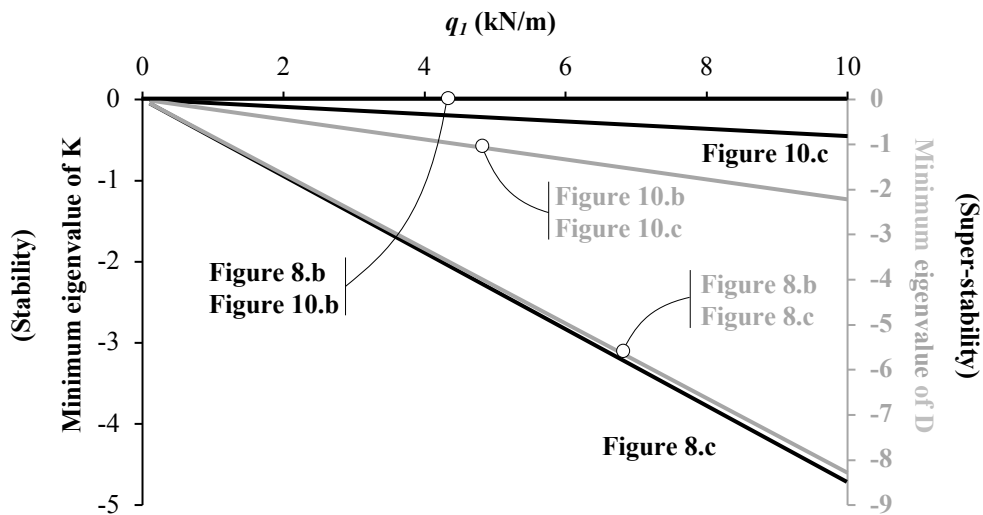


Figure 11. Study of stability and super-stability of the intermediate equilibrium configurations between the octahedron and the expanded octahedron (Figure 8.b and 8.c) and between the expanded octahedron and the double-expanded octahedron (Figure 10.b and 10.c).

The former results show that the more overlapped bars exist, the worse the stability is in the equilibrium configuration of the tensegrity (Gil-Martín et al., 2017a).

5. Conclusions

The first three members of the so-called octahedron family of tensegrities have been presented. The octahedron and the expanded octahedron are well-known examples of tensegrity structures. However, the double-expanded octahedron was not obtained until now. Both, the expanded and the double-expanded octahedrons have been obtained following some connectivity pattern rules presented in this work. Some simplifications in the value of the force:length ratio of each member have been introduced based on symmetry. The system of equations has been solved analytically, obtaining both full and folded forms. It has been proved that both, the octahedron and the expanded octahedron, are folded forms of the double-expanded octahedron (full form) proving that the latter is the third component of the family.

Acknowledgements

The authors would like to acknowledge the financial support provided by the University of Granada in the form of a Contrato Puente (postdoctoral fellowship) to the first author.

Appendix A (Adapted from Zhang & Ohsaki, 2015).

A.1. Relevant steps from Eq. (5) to Eq. (11) in Section 2.3: Stability of tensegrity structures

According to Eq. (5) the deformation energy associated with a differential deformation of a tensegrity with n nodes and dimension d can be approximated using a Taylor series expansion in displacements as:

$$\Delta\Gamma_{st} \approx \sum_{i=1}^{dn} \frac{\partial\Gamma_{st}}{\partial\delta_i} d\delta_i + \frac{1}{2} \sum_{i=1}^{dn} \sum_{j=1}^{dn} \frac{\partial^2\Gamma_{st}}{\partial\delta_i\partial\delta_j} d\delta_i d\delta_j \quad (\text{A1})$$

being δ the vector of nodal coordinates and Γ_{st} the elastic potential energy of a discrete structure with m members, defined as (Eq. (6) and Eq. (4) of the paper, respectively):

$$\delta^T = \{x_1, \dots, x_n, y_1, \dots, y_n, z_1, \dots, z_n\} \quad (\text{A2})$$

$$\Gamma_{st} = \frac{1}{2} \sum_{k=1}^m \frac{E_k \cdot \Omega_k \cdot (L_k - L_k^0)^2}{L_k^0} \quad (\text{A3})$$

Regarding the first term of Eq. (A1), substituting Eq. (A3) and accounting Eq. (3) of the paper it can be rewritten as:

$$\begin{aligned} \sum_{i=1}^{dn} \frac{\partial\Gamma_{st}}{\partial\delta_i} d\delta_i &= \sum_{i=1}^{dn} \frac{1}{2} \frac{\partial \left(\sum_{k=1}^m \frac{E_k \cdot \Omega_k \cdot (L_k - L_k^0)^2}{L_k^0} \right)}{\partial\delta_i} d\delta_i = \\ &= \sum_{i=1}^{dn} \left(\sum_{k=1}^m \frac{E_k \cdot \Omega_k \cdot (L_k - L_k^0)}{L_k^0} \frac{\partial L_k}{\partial\delta_i} \right) d\delta_i = \sum_{i=1}^{dn} \left(\sum_{k=1}^m N_k \frac{\partial L_k}{\partial\delta_i} \right) d\delta_i \end{aligned} \quad (\text{A4})$$

The sum between brackets in Eq. (A4) can be expressed in matrix form as:

$$\sum_{k=1}^m N_k \frac{\partial L_k}{\partial \delta_i} = \left(\frac{\partial L_1}{\partial \delta_i}, \frac{\partial L_2}{\partial \delta_i}, \dots, \frac{\partial L_m}{\partial \delta_i} \right) \begin{pmatrix} N_1 \\ \vdots \\ N_k \\ \vdots \\ N_m \end{pmatrix} = \Psi \cdot \mathbf{N} \quad (\text{A5})$$

being the matrix Ψ :

$$\Psi = \begin{pmatrix} \frac{\partial L_1}{\partial \delta_1} & \dots & \frac{\partial L_k}{\partial \delta_1} & \dots & \frac{\partial L_m}{\partial \delta_1} \\ \vdots & & \vdots & & \vdots \\ \frac{\partial L_1}{\partial \delta_i} & \dots & \frac{\partial L_k}{\partial \delta_i} & \dots & \frac{\partial L_m}{\partial \delta_i} \\ \vdots & & \vdots & & \vdots \\ \frac{\partial L_1}{\partial \delta_{dn}} & \dots & \frac{\partial L_k}{\partial \delta_{dn}} & \dots & \frac{\partial L_m}{\partial \delta_{dn}} \end{pmatrix} \quad (\text{A6})$$

According to the Euclidian distance, the vector length of the members is related with the vectors of nodal coordinates by (see Eq. (A6)):

$$\mathbf{L}^2 = \mathbf{U}^2 + \mathbf{V}^2 + \mathbf{Z}^2 \quad (\text{or } \mathbf{L}\mathbf{l} = \mathbf{U}\mathbf{u} + \mathbf{V}\mathbf{v} + \mathbf{Z}\mathbf{z}) \quad (\text{A7})$$

being \mathbf{l} the vector containing the length of the members and

$$\begin{aligned} \mathbf{L} &= \text{diag}(\mathbf{l}) \\ \mathbf{U} &= \text{diag}(\mathbf{u}) \quad \text{with } \mathbf{u} = \mathbf{C}\mathbf{x} \\ \mathbf{V} &= \text{diag}(\mathbf{v}) \quad \text{with } \mathbf{v} = \mathbf{C}\mathbf{y} \\ \mathbf{W} &= \text{diag}(\mathbf{w}) \quad \text{with } \mathbf{w} = \mathbf{C}\mathbf{z} \end{aligned} \quad (\text{A8})$$

Deriving Eq. (A7) and accounting (A8):

$$\begin{aligned} 2\mathbf{L} \frac{\partial \mathbf{L}}{\partial \delta_i} &= 2\mathbf{U} \frac{\partial \mathbf{U}}{\partial \delta_i} + 2\mathbf{V} \frac{\partial \mathbf{V}}{\partial \delta_i} + 2\mathbf{W} \frac{\partial \mathbf{W}}{\partial \delta_i} \Rightarrow \\ \Rightarrow \frac{\partial \mathbf{l}}{\partial \delta_i} &= \mathbf{L}^{-1} \mathbf{U} \frac{\partial \mathbf{u}}{\partial \delta_i} + \mathbf{L}^{-1} \mathbf{V} \frac{\partial \mathbf{v}}{\partial \delta_i} + \mathbf{L}^{-1} \mathbf{W} \frac{\partial \mathbf{w}}{\partial \delta_i} \Rightarrow \\ \Rightarrow \frac{\partial \mathbf{l}^T}{\partial \delta_i} &= \frac{\partial \mathbf{u}^T}{\partial \delta_i} \mathbf{U} \mathbf{L}^{-1} + \frac{\partial \mathbf{v}^T}{\partial \delta_i} \mathbf{V} \mathbf{L}^{-1} + \frac{\partial \mathbf{w}^T}{\partial \delta_i} \mathbf{W} \mathbf{L}^{-1} \end{aligned} \quad (\text{A9})$$

Because (see Eq. (A8)):

$$\frac{\partial \mathbf{u}^T}{\partial \delta_i} = \frac{\partial \mathbf{x}^T}{\partial \delta_i} \mathbf{C}^T \quad \text{and} \quad \frac{\partial \mathbf{v}^T}{\partial \delta_i} = \frac{\partial \mathbf{y}^T}{\partial \delta_i} \mathbf{C}^T \quad \text{and} \quad \frac{\partial \mathbf{w}^T}{\partial \delta_i} = \frac{\partial \mathbf{z}^T}{\partial \delta_i} \mathbf{C}^T \quad (\text{A10})$$

and accounting that the coordinate difference vector in x -direction \mathbf{u} is independent of both y and z coordinates (and analogously \mathbf{v} is independent of x and z and \mathbf{w} is independent of x and y), Eq. (A9) can be written as:

$$\begin{aligned}\frac{\partial \Gamma}{\partial \delta_i} &= \mathbf{C}^\top \mathbf{U} \mathbf{L}^{-1} \text{ if } \delta_i = x_i \\ \frac{\partial \Gamma}{\partial \delta_i} &= \mathbf{C}^\top \mathbf{V} \mathbf{L}^{-1} \text{ if } \delta_i = y_i \\ \frac{\partial \Gamma}{\partial \delta_i} &= \mathbf{C}^\top \mathbf{W} \mathbf{L}^{-1} \text{ if } \delta_i = z_i\end{aligned}\tag{A11}$$

Going back to the matrix Ψ defined in (A6), it is evident that the i row of Ψ can be expressed as:

$$\Psi_i = \frac{\partial \Gamma}{\partial \delta_i}\tag{A12}$$

And according to Eq. (A16) and the definition of the equilibrium matrix \mathbf{A} in Eq. (7) of the paper, matrix Ψ can be expressed as:

$$\Psi = \begin{pmatrix} \mathbf{C}^\top \mathbf{U} \mathbf{L}^{-1} \\ \mathbf{C}^\top \mathbf{V} \mathbf{L}^{-1} \\ \mathbf{C}^\top \mathbf{W} \mathbf{L}^{-1} \end{pmatrix} = \begin{pmatrix} \mathbf{C}^\top \text{diag}(\mathbf{C}\mathbf{x}) \\ \mathbf{C}^\top \text{diag}(\mathbf{C}\mathbf{y}) \\ \mathbf{C}^\top \text{diag}(\mathbf{C}\mathbf{z}) \end{pmatrix} \mathbf{L}^{-1} = \mathbf{A} \mathbf{L}^{-1}\tag{A13}$$

Introducing (A13) in (A5) gives:

$$\sum_{k=1}^m N_k \frac{\partial L_k}{\partial \delta_i} = \Psi \cdot \mathbf{N} = \mathbf{A} \mathbf{L}^{-1} \mathbf{N} = \mathbf{A} \cdot \mathbf{q} = \mathbf{0}\tag{A14}$$

The former expression corresponds to the equilibrium of the tensegrity and vanishes (see Eq. (7) of the paper).

Regarding the second term of Eq. (A1), it can be rewritten as:

$$\frac{1}{2} \sum_{i=1}^{dn} \sum_{j=1}^{dn} \frac{\partial^2 \Gamma}{\partial \delta_i \partial \delta_j} d\delta_i d\delta_j = \frac{1}{2} d\delta^\top \mathbf{K} d\delta\tag{A15}$$

Where \mathbf{K} is a matrix ($dn \times dn$) whose entry ij is $K_{ij} = \frac{\partial^2 \Gamma_{st}}{\partial \delta_i \partial \delta_j}$. Henceforth by convenience and without

loss of generality $\frac{\partial}{\partial \delta_i} \left(\frac{\partial \Gamma_{st}}{\partial \delta_j} \right)^\top$ is going to be considered instead of $\frac{\partial}{\partial \delta_i} \left(\frac{\partial \Gamma_{st}}{\partial \delta_j} \right)$. Accounting Eq. (A14)

and Eq. (10) of the paper:

$$\begin{aligned} \mathbf{K} &= \frac{\partial}{\partial \delta} \left(\frac{\partial \Gamma_{st}}{\partial \delta} \right)^\top = \frac{\partial}{\partial \delta} (\mathbf{A} \cdot \mathbf{q})^\top = \frac{\partial}{\partial \delta} \begin{pmatrix} \mathbf{D} \cdot \mathbf{x} \\ \mathbf{D} \cdot \mathbf{y} \\ \mathbf{D} \cdot \mathbf{z} \end{pmatrix}^\top = \begin{pmatrix} \frac{\partial(\mathbf{x}^\top \mathbf{D})}{\partial \delta} & \frac{\partial(\mathbf{y}^\top \mathbf{D})}{\partial \delta} & \frac{\partial(\mathbf{z}^\top \mathbf{D})}{\partial \delta} \end{pmatrix} = \\ &= \begin{pmatrix} \frac{\partial(\mathbf{x}^\top \mathbf{D})}{\partial \mathbf{x}} & \frac{\partial(\mathbf{y}^\top \mathbf{D})}{\partial \mathbf{x}} & \frac{\partial(\mathbf{z}^\top \mathbf{D})}{\partial \mathbf{x}} \\ \frac{\partial(\mathbf{x}^\top \mathbf{D})}{\partial \mathbf{y}} & \frac{\partial(\mathbf{y}^\top \mathbf{D})}{\partial \mathbf{y}} & \frac{\partial(\mathbf{z}^\top \mathbf{D})}{\partial \mathbf{y}} \\ \frac{\partial(\mathbf{x}^\top \mathbf{D})}{\partial \mathbf{z}} & \frac{\partial(\mathbf{y}^\top \mathbf{D})}{\partial \mathbf{z}} & \frac{\partial(\mathbf{z}^\top \mathbf{D})}{\partial \mathbf{z}} \end{pmatrix} \end{aligned} \quad (\text{A16})$$

Let us consider one of the 3×3 submatrices of the diagonal of the matrix \mathbf{K} above, for example \mathbf{K}_{11} :

$$\mathbf{K}_{11} = \frac{\partial(\mathbf{x}^\top \mathbf{D})}{\partial \mathbf{x}} = \frac{\partial \mathbf{x}^\top}{\partial \mathbf{x}} \mathbf{D} + \sum_{i=1}^n \frac{\partial \mathbf{D}}{\partial x_i} x_i = \mathbf{D} + \sum_{i=1}^n \frac{\partial \mathbf{D}}{\partial x_i} x_i \quad (\text{A17})$$

Accounting the definition of the force density matrix, Eq. (3) of the paper and Eqs. (A8) and (A9):

$$\begin{aligned} \mathbf{D} &= \mathbf{C}^\top \mathbf{Q} \mathbf{C} = \mathbf{C}^\top \text{diag} \left(\Omega E \left(\frac{1}{\mathbf{L}_0} - \frac{1}{\mathbf{L}} \right) \right) \mathbf{C} \Rightarrow \\ \frac{\partial \mathbf{D}}{\partial x_i} &= \mathbf{C}^\top \frac{\partial \mathbf{Q}}{\partial x_i} \mathbf{C} = \mathbf{C}^\top \left(\Omega E \frac{1}{\mathbf{L}^2} \frac{\partial \mathbf{L}}{\partial x_i} \right) \mathbf{C} = \mathbf{C}^\top \left(\Omega E \frac{1}{\mathbf{L}^2} \mathbf{L}^1 \mathbf{U} \frac{\partial \mathbf{U}}{\partial x_i} \right) \mathbf{C} \end{aligned} \quad (\text{A18})$$

being the first derivative of \mathbf{U} :

$$\frac{\partial \mathbf{U}}{\partial x_i} = \text{diag} \left(\mathbf{C} \frac{\partial \mathbf{x}}{\partial x_i} \right) = \text{diag} (\mathbf{C}_{col,i}) \quad (\text{A19})$$

Where $\mathbf{C}_{col,i}$ denotes the i column of the connectivity matrix \mathbf{C} . Introducing Eq. (A19) into Eq. (A18):

$$\frac{\partial \mathbf{D}}{\partial x_i} = \mathbf{C}^\top \left(\Omega E \frac{1}{\mathbf{L}^2} \mathbf{L}^1 \mathbf{U} \frac{\partial \mathbf{U}}{\partial x_i} \right) \mathbf{C} = \mathbf{C}^\top \left(\Omega E \frac{1}{\mathbf{L}^3} \mathbf{U} \text{diag} (\mathbf{C}_{col,i}) \right) \mathbf{C} \quad (\text{A20})$$

Introducing Eq. (A20) into Eq. (A17) and accounting the definition of the equilibrium matrix in Eq. (7)

of the paper, the following is obtained:

$$\begin{aligned}
\mathbf{K}_{11} &= \frac{\partial(\mathbf{x}^\top \mathbf{D})}{\partial \mathbf{x}} = \frac{\partial \mathbf{x}^\top}{\partial \mathbf{x}} \mathbf{D} + \sum_{i=1}^n \frac{\partial \mathbf{D}}{\partial x_i} x_i = \mathbf{D} + \mathbf{C}^\top \left(\Omega E \frac{1}{\mathbf{L}^3} \mathbf{U} \text{diag} \left(\sum_{i=1}^n (\mathbf{C}_{col,i} x_i) \right) \right) \mathbf{C} = \\
&= \mathbf{D} + \mathbf{C}^\top \left(\Omega E \frac{1}{\mathbf{L}^3} \mathbf{U} \text{diag}(\mathbf{C} \mathbf{x}) \right) \mathbf{C} = \mathbf{D} + \mathbf{C}^\top \left(\Omega E \frac{1}{\mathbf{L}^3} \mathbf{U} \mathbf{U} \right) \mathbf{C} = \mathbf{D} + \mathbf{A}_x \text{diag} \left(\Omega E \frac{1}{\mathbf{L}^3} \right) \mathbf{A}_x^\top
\end{aligned} \tag{A21}$$

being $\mathbf{A}_x = \mathbf{C}^\top \text{diag}(\mathbf{C} \cdot \mathbf{x})$.

Analogously:

$$\mathbf{K}_{22} = \mathbf{D} + \mathbf{A}_y \text{diag} \left(\Omega E \frac{1}{\mathbf{L}^3} \right) \mathbf{A}_y^\top \quad \text{and} \quad \mathbf{K}_{33} = \mathbf{D} + \mathbf{A}_z \text{diag} \left(\Omega E \frac{1}{\mathbf{L}^3} \right) \mathbf{A}_z^\top \tag{A22}$$

Let us now consider now any of the 3×3 submatrices out of the diagonal of the matrix \mathbf{K} (Eq. (A16)),

such \mathbf{K}_{12} :

$$\mathbf{K}_{12} = \frac{\partial(\mathbf{y}^\top \mathbf{D})}{\partial \mathbf{x}} = \frac{\partial \mathbf{y}^\top}{\partial \mathbf{x}} \mathbf{D} + \sum_{i=1}^n \frac{\partial \mathbf{D}}{\partial x_i} y_i = \mathbf{O}_{n \times n} + \sum_{i=1}^n \frac{\partial \mathbf{D}}{\partial x_i} y_i \tag{A23}$$

being $\mathbf{O}_{n \times n}$ the zero matrix $n \times n$ dimension. In a similar way to how it was done in Eq. (A21), the

following expressions can be obtained for the entries of the matrix \mathbf{K} :

$$\begin{aligned}
\mathbf{K}_{12} &= \mathbf{A}_x \text{diag} \left(\Omega E \frac{1}{\mathbf{L}^3} \right) \mathbf{A}_y^\top & \mathbf{K}_{13} &= \mathbf{A}_x \text{diag} \left(\Omega E \frac{1}{\mathbf{L}^3} \right) \mathbf{A}_z^\top \\
\mathbf{K}_{21} &= \mathbf{A}_y \text{diag} \left(\Omega E \frac{1}{\mathbf{L}^3} \right) \mathbf{A}_x^\top & \mathbf{K}_{23} &= \mathbf{A}_y \text{diag} \left(\Omega E \frac{1}{\mathbf{L}^3} \right) \mathbf{A}_z^\top \\
\mathbf{K}_{31} &= \mathbf{A}_z \text{diag} \left(\Omega E \frac{1}{\mathbf{L}^3} \right) \mathbf{A}_x^\top & \mathbf{K}_{32} &= \mathbf{A}_z \text{diag} \left(\Omega E \frac{1}{\mathbf{L}^3} \right) \mathbf{A}_y^\top
\end{aligned} \tag{A24}$$

Accounting Eqs. from (A17) to (A24), the matrix \mathbf{K} in Eq. (A16) can be re-written as:

$$\mathbf{K} = \mathbf{I}_d \otimes \mathbf{D} + \mathbf{A} \text{diag} \left(\frac{\Omega E}{\mathbf{L}^3} \right) \mathbf{A}^\top = \mathbf{K}_{\text{Geom}} + \mathbf{K}_{\text{Elast}} \tag{A25}$$

where the symbol \otimes denotes the Kronecker product.

A.2. Compatibility matrix

Let $\boldsymbol{\delta} \in \mathfrak{R}^{dn}$ the vector of infinitesimal nodal displacements due to the external load \mathbf{p} applied to the structure and let $\boldsymbol{\Delta} \ell \in \mathfrak{R}^m$ the vector containing the variations of lengths of the members. Both vectors are related by the kinematic relations in terms of the compatibility matrix $\mathbf{S} \in \mathfrak{R}^{m \times dn}$:

$$\mathbf{S} \boldsymbol{\delta} = \boldsymbol{\Delta} \ell \tag{A26}$$

Applying the principle of virtual work (the virtual work done by the external loads is equal to virtual internal work done by member forces) for the arbitrary virtual displacements $\Delta\delta$ and their corresponding virtual member extensions $\Delta(\Delta\ell)$ the following equation is satisfied:

$$\mathbf{p}^\top(\Delta\delta) = \mathbf{N}^\top(\Delta(\Delta\ell)) \quad (\text{A27})$$

Being $\mathbf{N} \in \mathfrak{R}^m$ the vector containing the axial force of each member of the structure. Accounting Eq. (A26), Eq. (A27) can be re-written:

$$\mathbf{p}^\top(\Delta\delta) = \mathbf{N}^\top(\mathbf{S}\Delta\delta) = \mathbf{N}^\top\mathbf{S}(\Delta\delta) \quad (\text{A28})$$

Accounting for the relationship between the vector of external loads \mathbf{p} and the vector of axial load or prestresses, \mathbf{N} (or equivalently the one of force-length ratio coefficients $\mathbf{q} = \mathbf{L}^{-1}\mathbf{N}$ being $\mathbf{L} = \text{diag}(\mathbf{l})$ being \mathbf{l} the vector containing the length of the members), in Eq. (A28):

$$\mathbf{A}\mathbf{q} = \mathbf{p} \rightarrow \mathbf{p}^\top = \mathbf{q}^\top\mathbf{A}^\top$$

(A29)

being $\mathbf{A} = \begin{pmatrix} \mathbf{C}^\top \text{diag}(\mathbf{C} \cdot \mathbf{x}) \\ \mathbf{C}^\top \text{diag}(\mathbf{C} \cdot \mathbf{y}) \\ \mathbf{C}^\top \text{diag}(\mathbf{C} \cdot \mathbf{z}) \end{pmatrix}$ the equilibrium matrix of the structure (Eq. (7) of the paper).

Combining Eqs. (A28) and (A29) the following expression for the compatibility matrix is obtained:

$$\mathbf{q}^\top\mathbf{A}^\top = \mathbf{N}^\top\mathbf{S} \rightarrow \mathbf{S} = (\mathbf{L}^{-1})^\top \mathbf{A}^\top \quad (\text{A30})$$

A.3. Geometry matrix.

The matrix $\mathbf{G} \in \mathfrak{R}^{m \times d(d+1)/2}$ is called the *geometry matrix* because it is only related to the geometry of the structure. It is defined as:

$$\mathbf{G} = (\mathbf{Uu}, \mathbf{Vv}, \mathbf{Ww}, \mathbf{Uv}, \mathbf{Uw}, \mathbf{Vw}) \quad (\text{A31})$$

Appendix B. Polynomials a_1 , a_2 and a_3

For the octahedron presented in Section 4.1 the polynomials a_1 , a_2 and a_3 of its corresponding characteristic polynomial $p(\lambda) = \lambda^n + a_{n-1}\lambda^{n-1} + \dots + a_3\lambda^3 + a_2\lambda^2 + a_1\lambda + a_0$ are the following:

$$a_1 = -2304q_1^5 - 3456q_1^4q_2 - 1728q_1^3q_2^2 - 288q_1^2q_2^3 \quad (\text{B1})$$

$$a_2 = 2496q_1^4 + 2880q_1^3q_2 + 1008q_1^2q_2^2 + 96q_1q_2^3 \quad (\text{B2})$$

$$a_3 = -1072q_1^3 - 888q_1^2q_2 - 192q_1q_2^2 - 8q_2^3 \quad (\text{B3})$$

For the expanded octahedron presented in Section 4.2 the polynomials a_1 , a_2 and a_3 are the following:

$$\begin{aligned} a_1 = & -3981312q_1^{11} - 13934592q_1^{10}q_2 - 20238336q_1^9q_2^2 \\ & - 15611904q_1^8q_2^3 - 6746112q_1^7q_2^4 - 1548288q_1^6q_2^5 \\ & - 147456q_1^5q_2^6 \end{aligned} \quad (\text{B4})$$

$$\begin{aligned} a_2 = & 12275712q_1^{10} + 38154240q_1^9q_2 + 48522240q_1^8q_2^2 \\ & + 32188416q_1^7q_2^3 + 11676672q_1^6q_2^4 + 2174976q_1^5q_2^5 \\ & + 159744q_1^4q_2^6 \end{aligned} \quad (\text{B5})$$

$$\begin{aligned} a_3 = & -16782336q_1^9 - 45826560q_1^8q_2 - 50374656q_1^7q_2^2 \\ & - 28284416q_1^6q_2^3 - 8444928q_1^5q_2^4 - 1245696q_1^4q_2^5 \\ & - 68608q_1^3q_2^6 \end{aligned} \quad (\text{B6})$$

For the double-expanded octahedron presented in Section 4.3 the polynomials a_1 , a_2 and a_3 are the following:

$$\begin{aligned} a_1 = & -8349416423424q_1^{23} - 60533269069824q_1^{22}q_2 - 200559940337664q_1^{21}q_2^2 \\ & - 401549914275840q_1^{20}q_2^3 - 541088569884672q_1^{19}q_2^4 - 516971657428992q_1^{18}q_2^5 \\ & - 359110671335424q_1^{17}q_2^6 - 182742234955776q_1^{16}q_2^7 - 67612516024320q_1^{15}q_2^8 \\ & - 17738357538816q_1^{14}q_2^9 - 3132390113280q_1^{13}q_2^{10} - 334302806016q_1^{12}q_2^{11} \\ & - 16307453952q_1^{11}q_2^{12} \end{aligned} \quad (\text{B7})$$

$$\begin{aligned} a_2 = & 63316407877632q_1^{22} + 434865438720000q_1^{21}q_2 + 1361607175176192q_1^{20}q_2^2 \\ & + 2569393586307072q_1^{19}q_2^3 + 3253498930003968q_1^{18}q_2^4 + 2911356466495488q_1^{17}q_2^5 \\ & + 1887017537372160q_1^{16}q_2^6 + 892190620385280q_1^{15}q_2^7 + 305210459160576q_1^{14}q_2^8 \\ & + 73618616745984q_1^{13}q_2^9 + 11873525170176q_1^{12}q_2^{10} + 1148316549120q_1^{11}q_2^{11} \\ & + 50281316352q_1^{10}q_2^{12} \end{aligned} \quad (\text{B8})$$

$$\begin{aligned}
a_3 = & -224622494613504q_1^{21}-1458190789115904q_1^{20}q_2-4304171276697600q_1^{19}q_2^2 \\
& -7634456135335936q_1^{18}q_2^3-9057178849640448q_1^{17}q_2^4-7565602524758016q_1^{16}q_2^5 \\
& -4558609274896384q_1^{15}q_2^6-1994215749844992q_1^{14}q_2^7-627786821664768q_1^{13}q_2^8 \\
& -138469760303104q_1^{12}q_2^9-20270957985792q_1^{11}q_2^{10}-1763753066496q_1^{10}q_2^{11} \\
& -68740448256q_1^9q_2^{12}
\end{aligned} \tag{B9}$$

Appendix C. Supplementary data

Supplementary data associated with this article can be found in the web version of this article.

References

- Adam, B., Smith, I.F.C., 2008. Active tensegrity: A control framework for an adaptive civil-engineering structure. *Comput. Struct.* 86, 2215–2223.
<https://doi.org/10.1016/j.compstruc.2008.05.006>
- Bel Hadj Ali, N., Rhode-Barbarigos, L., Smith, I.F.C., 2011. Analysis of clustered tensegrity structures using a modified dynamic relaxation algorithm. *Int. J. Solids Struct.* 48, 637–647.
<https://doi.org/10.1016/j.ijsolstr.2010.10.029>
- Estrada, G.G., Bungartz, H.-J., Mohrdieck, C., 2006. Numerical form-finding of tensegrity structures. *Int. J. Solids Struct.* 43, 6855–6868.
- Fernández-Ruiz, M.A., Hernández-Montes, E., Carbonell-Márquez, J.F., Gil-Martín, L.M., 2017. Patterns of force:length ratios for the design of compression structures with inner ribs. *Eng. Struct.* 148, 878–889. <https://doi.org/10.1016/j.engstruct.2017.07.027>
- Fuller, R.B., 1975. *Synergetics - explorations in the geometry of thinking*. Macmillan, London, UK.
- Gil-Martín, L.M., Fernández-Ruiz, M.A., Carbonell-Márquez, J.F., 2017a. Families of free-standing pre-stressed pin-jointed structures. Some remarks on stability, in: *4th International Conference on Mechanical Models in Structural Engineering*. Madrid (Spain), pp. 343–360.
- Gil-Martín, L.M., Fernández-Ruiz, M.A., Hernández-Montes, E., 2017b. A necessary discussion on the

- stiffness matrices used in tensegrity structures. *J. Appl. Eng. Sci.* 15, 383–388.
<https://doi.org/10.5937/jaes15-14766>
- Graells Rovira, A., Mirats Tur, J.M., 2009. Control and simulation of a tensegrity-based mobile robot. *Rob. Auton. Syst.* 57, 526–535. <https://doi.org/10.1016/j.robot.2008.10.010>
- Hernández-Montes, E., Fernández-Ruiz, M.A., Gil-Martín, L.M., Merino, L., Jara, P., 2017. Full and folded forms: a compact review of the formulation of tensegrity structures. *Math. Mech. Solids*.
- Hernández-Montes, E., Jurado-Piña, R., Bayo, E., 2006. Topological Mapping for Tension Structures. *J. Struct. Eng.* 132, 970–977. [https://doi.org/10.1061/\(ASCE\)0733-9445\(2006\)132:6\(970\)](https://doi.org/10.1061/(ASCE)0733-9445(2006)132:6(970))
- Ingber, D.E., 1998. The Architecture of Life. *Sci. Am.* 278, 48–57.
- Jurado-Piña, R., Gil-Martín, L.M., Hernández-Montes, E., 2009. Topological mesh for shell structures. *Appl. Math. Model.* 33, 948–958. <https://doi.org/10.1016/j.apm.2007.12.018>
- Levy, R., Spillers, W.R., 2004. Analysis of geometrically nonlinear structures, 2nd Ed. ed. Chapman & Hall, London.
- Linkwitz, K., Schek, H.J., 1971. Einige Bemerkungen zur Berechnung von vorgespannten Seilnetzkonstruktionen. *Ingenieur-Archiv.* 40, 145–158.
- Masic, M., Skelton, R.E., Gill, P.E., 2005. Algebraic tensegrity form-finding. *Int. J. Solids Struct.* 42, 4833–4858. <https://doi.org/10.1016/j.ijsolstr.2005.01.014>
- Otter, J.R.H., 1965. Computations for prestressed concrete reactor pressure vessels using dynamic relaxation. *Nucl. Struct. Eng.* 1, 61–75. [https://doi.org/10.1016/0369-5816\(65\)90097-9](https://doi.org/10.1016/0369-5816(65)90097-9)
- Pugh, A., 1976. An introduction to tensegrity. University of California Press.
- Schek, H.J., 1974. The force density method for form-finding and computation of general networks. *Comput. Methods Appl. Mech. Eng.* 3, 115–134.
- Tibert, A.G., Pellegrino, S., 2003. Review of Form-Finding Methods for Tensegrity Structures. *Int. J. Sp. Struct.* 18, 209–223.
- Tibert, A.G., Pellegrino, S., 2002. Deployable Tensegrity Reflectors for Small Satellites. *J. Spacecr.*

- Rockets 39, 701–709. <https://doi.org/10.2514/2.3867>
- Tran, H.C., Lee, J., 2010. Advanced form-finding of tensegrity structures. *Comput. Struct.* 88, 237–246. <https://doi.org/10.1016/j.compstruc.2009.10.006>
- Vassart, N., Motro, R., 1999. Multiparametered form-finding method: application to tensegrity systems. *Int. J. Sp. Struct.* 14, 89–104.
- Xu, X., Luo, Y., 2011. Multistable Tensegrity Structures. *J. Struct. Eng.* 137, 117–123. [https://doi.org/10.1061/\(ASCE\)ST.1943-541X.0000281](https://doi.org/10.1061/(ASCE)ST.1943-541X.0000281)
- Zhang, J.Y., Ohsaki, M., 2015. *Tensegrity Structures. Form, Stability, and Symmetry.* Springer.
- Zhang, J.Y., Ohsaki, M., 2007. Stability conditions for tensegrity structures. *Int. J. Solids Struct.* 44, 3875–3886. <https://doi.org/10.1016/j.ijsolstr.2006.10.027>
- Zhang, J.Y., Ohsaki, M., 2006. Adaptive force density method for form-finding problem of tensegrity structures. *Int. J. Solids Struct.* 43, 5658–5673. <https://doi.org/10.1016/j.ijsolstr.2005.10.011>
- Zhang, L., Maurin, B., Motro, R., 2006. Form-Finding of Nonregular Tensegrity Systems. *J. Struct. Eng.* 132, 1435–1440. [https://doi.org/10.1061/\(ASCE\)0733-9445\(2006\)132:9\(1435\)](https://doi.org/10.1061/(ASCE)0733-9445(2006)132:9(1435))
- Zhang, L.Y., Li, Y., Cao, Y.P., Feng, X.Q., 2013. A unified solution for self-equilibrium and super-stability of rhombic truncated regular polyhedral tensegrities. *Int. J. Solids Struct.* 50, 234–245. <https://doi.org/10.1016/j.ijsolstr.2012.09.024>